INSTITUTE OF PHYSICS PUBLISHING PLASMA PHYSICS AND CONTROLLED FUSION

Plasma Phys. Control. Fusion **46** (2004) 471–487 PII: S0741-3335(04)69034-8

Plasma species mix diagnostic using ion–ion hybrid layer reflectometry

G W Watson[1], W W Heidbrink[1], K H Burrell[2] and G J Kramer[3]

[1] University of California, Irvine, California, USA
[2] General Atomics, San Diego, California, USA
[3] Princeton Plasma Physics Laboratory, Princeton, New Jersey, USA

Received 16 September 2003
Published 4 February 2004
Online at stacks.iop.org/PPCF/46/471 (DOI: 10.1088/0741-3335/46/3/004)

Abstract

A superheterodyne reflectometer could provide a direct and inexpensive measurement of ion species mixes with different charge-to-mass ratios. Using the cold plasma dispersion relation, the ion–ion hybrid cutoff frequency is uniquely determined by the density ratio and cyclotron frequencies of the two different species. The phase of a 20 MHz wave that travels from the launching point to the cutoff layer to the receiving antenna provides a direct measure of the hydrogen : deuterium species mix. In the first experiment, a fast Alfvén wave is launched perpendicular to a hydrogen–deuterium plasma from the low field side of the DIII-D tokamak. Quantitative measurements observe a hydrogen concentration range of 3–67% and a maximum penetration depth of 0.60 m. Corroborative values are obtained from two independent diagnostics. In the second experiment, the fast Alfvén wave is launched from the high field side (HFS) during a hydrogen puffing experiment. The results suggest that a wave launched from the HFS is able to tunnel through the resonance layer and reflect back to the receiving antenna.

1. Introduction

Ion species measurements in a tokamak plasma have several benefits. A direct measure of the ion species mix in the interior of the plasma can be utilized to help achieve and maintain a deuterium and tritium density equilibrium ($n_D \simeq n_T$), maximizing fusion reactions in a burning plasma experiment. A number of wave heating schemes in the ion cyclotron range of frequencies (ICRF) depend on the relative concentrations of ions with different charge-to-mass ratios, and so measurements of the concentrations are required to understand and control the heating profile. In transport studies, measurement of the density profiles of ions with different charge-to-mass ratios can help illuminate the mechanisms of particle transport.

Several methods to measure the ion species mix exist. One method uses the H_α, D_α, and T_α light emitted from hydrogenic atoms [1, 2]. However, a Balmer-alpha diagnostic can only

make a species mix measurement of neutral hydrogen, which is generally concentrated at the plasma boundary; interior activity goes undetected. Another method detects neutral particles that undergo charge exchange reactions in the plasma and escape to a mass-resolving neutral-particle analyser [3, 4]. Although neutrals are rare in the core of a hot plasma, injection of a modulated neutral beam can enhance the signal that originates in the core [5]. Insufficient penetration of the injected and escaping neutrals may limit the applicability of this technique in a reactor plasma [6], although possible solutions are being evaluated [7]. Fusion reaction measurements can yield the density of one of the reactants [8], especially under transient conditions such as a neutral beam blip [9], an injected pellet [10], or a gas puff [8, 11]. Although all these techniques provide useful information, alternative techniques that provide direct measurements of the species mix inside the plasma are desirable.

Ikezi *et al* [12] proposed a reflectometer diagnostic that uses an ICRF wave to measure the ion species mix. With proper choice of frequency, this diagnostic can make a time-resolved measurement deep into the plasma. In addition, with the simplicity of design and commercialization in the radio frequency (RF) band, this reflectometer is a low-cost, practical way to make a species mix diagnostic with good temporal resolution.

This paper describes the first measurements of the hydrogen–deuterium species mix using ion–ion hybrid layer reflectometry in a tokamak plasma. Successful measurements from antennas mounted on both the outer wall and the inner wall are described. In cold plasma theory, the ion–ion hybrid cutoff frequency is uniquely determined by the density ratio and the cyclotron frequencies of the ion species (section 2). The reflectometer apparatus is described in section 3. Species mix measurements by the reflectometer system and two corroborating diagnostics are then presented (section 4). This paper concludes with an assessment of the merits and challenges of the technique (section 5).

2. Theory

In the case of the ion–ion species mix reflectometer diagnostic, a RF wave is launched perpendicular to the magnetic field. The ion species mix concentrations can be measured by calculating the time of flight for the wave as it travels from a launching antenna to the ion–ion hybrid cutoff layer (IIHCL) and then reflects back to a receiving antenna (figure 1). In the cold plasma approximation, the index of refraction, n, perpendicular to the magnetic field, $\boldsymbol{B}$, is given by $n^2 = RL/S$ in Stix's notation [13]. Cutoff occurs when $L = 0$ or $R = 0$; resonance occurs when $S = 0$. For two ion species in a quasineutral plasma, the ion–ion hybrid cutoff occurs for $L = 0$, which occurs when the wave frequency is

$$\omega_{\text{cutoff}} \simeq \Omega_1 f_2 + \Omega_2 f_1, \tag{1}$$

where Ω_1 and Ω_2 are the cyclotron frequencies of the two species, $\Omega_s = Z_s eB/m_s$, and f_1 and f_2 are the fraction of electrons, $q_{\text{i}} n_{\text{i}}/n_{\text{e}}$, neutralized by each species. The two species have different charge-to-mass ratios, Z/A. (All particles with the same charge-to-mass ratio are considered a 'species'.) In the case of a hydrogen–deuterium plasma where $A_{\text{D}} = 2A_{\text{H}}$, equation (1) takes the form

$$\omega_{\text{cutoff}} \simeq \Omega_{\text{H}}\left(1 - \tfrac{1}{2} f_{\text{H}}\right), \tag{2}$$

where f_{H} is the hydrogen concentration, $n_{\text{H}}/n_{\text{e}}$.

The ion–ion or Buchsbaum [14] resonance occurs in a two-ion species plasma when

$$\frac{\omega_{\text{p1}}^2}{\omega^2 - \Omega_1^2} + \frac{\omega_{\text{p2}}^2}{\omega^2 - \Omega_2^2} \simeq 0, \tag{3}$$

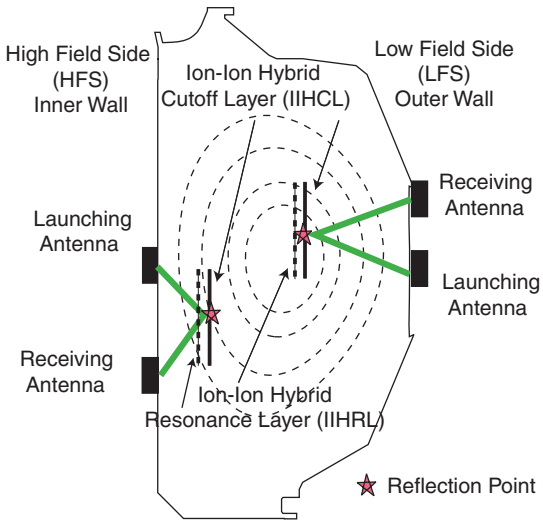

Figure 1. Elevation of DIII-D illustrating the basic concept. Waves are launched by graphite tile antennae near the midplane, reflect off the IIHCL, and are received by a nearby graphite tile antenna. Waves launched from the LFS encounter the cutoff layer prior to the ion–ion hybrid resonance layer. Waves launched from the HFS must tunnel through the resonance layer in order to reflect off the cutoff (refraction neglected). The dashed lines represent plasma flux surfaces.

where $\omega_{ps}^2 = 4\pi n_s q_s^2/m_s$ is the plasma frequency of species s. In a plasma composed of hydrogen and deuterium (and additional species with $Z_s/A_s = 1/2$), the resonance is at

$$\omega_{\text{resonance}} = \Omega_{\text{H}}\sqrt{\frac{1 - f_{\text{H}}/2}{1 + f_{\text{H}}}}. \tag{4}$$

The ion–ion hybrid resonant frequency is slightly lower than the ion–ion hybrid cutoff frequency, $\omega_{\text{resonance}} < \omega_{\text{cutoff}}$.

A tokamak plasma is inhomogeneous. The ion cyclotron frequency is a function of the magnetic field, which in turn is a function of the major radius, R, $B(R) \simeq B_0 R_0/R$, and so the cyclotron, cutoff, and resonance frequencies are functions of position (figure 2). The plasma density also varies spatially, causing additional inhomogeneities in the index of refraction, n. Consequently, the index of refraction changes rapidly with position (figure 3). Consider a wave launched from the outside of the torus within the context of WKB theory. A wave launched from the low field side (LFS) propagates until its frequency equals the cutoff frequency, where it is reflected back towards the outer wall. The propagation time (and associated phase) depends on the wave path and on the index of refraction along that path, $t \propto \int n\,\mathrm{d}l$. By measuring t, one can determine the radial position of the cutoff and hence the hydrogen concentration.

The situation is more complicated if the wave is launched from the inner wall. A wave launched from the high field side (HFS) propagates until its frequency equals the resonance frequency where, within the context of WKB, it is absorbed (figure 2). In practice, however, the spatial separation of the resonance and cutoff layers is short compared with a wavelength (figure 3), and so the cutoff and resonance layers form a couplet that is described by mode conversion theory [15]. In general, reflection, transmission, and mode conversion occur at the couplet layer. For a wave incident from the LFS, most of the energy is reflected; so the simple WKB description of the diagnostic is a useful approximation. For a wave incident from the HFS, transmission and mode conversion [16] are important, but some reflection is also

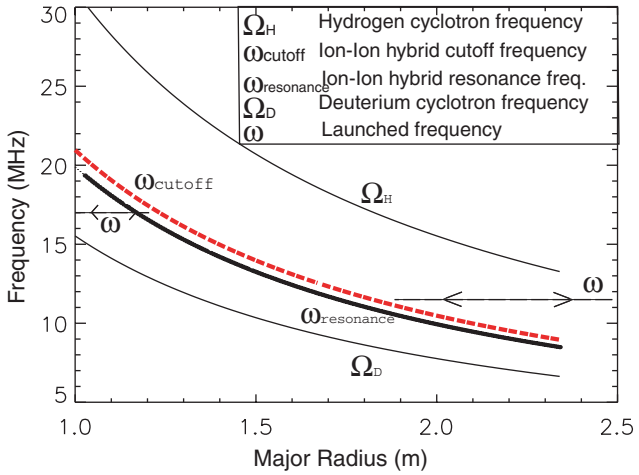

Figure 2. The ion–ion hybrid cutoff (grey dashed line) and ion–ion hybrid resonance (——) vs major radius, R, for $f_{\mathrm{H}} = 44\%$, $B = B_0 R_0/R$, and uniform density profiles. These curves lie between the deuterium and hydrogen cyclotron frequencies (——). Possible launch frequencies that reflect off the ion–ion cutoff layer are indicated by dashed lines with arrowheads. (Although the curves are labelled by angular frequencies, the ordinate is the frequency in megahertz.)

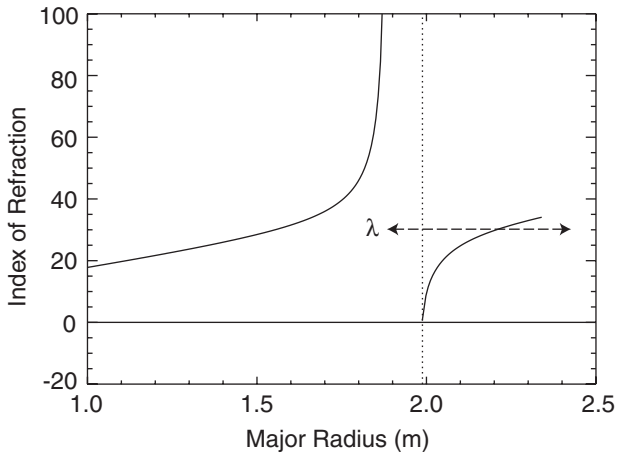

Figure 3. The index of refraction, n, vs major radius for a typical case. The cutoff layer occurs where $n = 0$ (· · · · · ·). The wavelength for $n = 30$ and $\omega/(2\pi) = 20\,\mathrm{MHz}$ is illustrated by the dashed line.

possible [17]. If the energy in the reflected wave is sufficient for detection, the position of the couplet layer can be inferred.

If the concentration of one species is small, fundamental cyclotron absorption by the minority species becomes important [18]. If the parallel wavelength is appreciable, an additional cutoff can enhance mode conversion [19]. Both these complications are avoided in our experiment. As an additional simplification, the waves launched in this experiment avoid the fundamental and second harmonic cyclotron frequencies.

An interesting and important point is that, as the hydrogen concentration increases, the ion–ion cutoff and resonance curves approach the deuterium cyclotron frequency. Likewise,

Table 1. Impact of changes in hydrogen concentration, f_H, on the observed reflectometer phase.

Hydrogen concentration	Cutoff approaches	Launch location	Phase	Polar-plot rotation
Increases	Ω_D	HFS	Decreases	Clockwise
Decreases	Ω_H	HFS	Increases	Counter-clockwise
Increases	Ω_D	LFS	Increases	Counter-clockwise
Decreases	Ω_H	LFS	Decreases	Clockwise

for a hydrogen concentration decrease, the cutoff and resonance curves approach the hydrogen cyclotron frequency. This behaviour affects the wave's path length as it travels in the tokamak. A summary of the ion–ion hybrid cutoff–resonance couplet and its relation to the observed phase change is given in table 1. All the predictions in table 1 are observed experimentally (section 4).

In the above discussion, only two ion species were considered. We now consider the impact of a third ion species with a different charge-to-mass ratio that neutralizes a fraction of the electrons f_3. Cutoffs occur when

$$\frac{f_1\Omega_1}{\Omega_1-\omega}+\frac{f_2\Omega_2}{\Omega_2-\omega}+\frac{f_3\Omega_3}{\Omega_3-\omega}-1\simeq 0 \tag{5}$$

and resonances occur when

$$\frac{f_1\Omega_1}{\omega^2-\Omega_1^2}+\frac{f_2\Omega_2}{\omega^2-\Omega_2^2}+\frac{f_3\Omega_3}{\omega^2-\Omega_3^2}\simeq 0. \tag{6}$$

The structure of equations (5) and (6) is evident: a hybrid cutoff or resonance occurs when some denominators are negative and others are positive. In other words, equations (5) and (6) can be satisfied for values of ω that fall between the cyclotron frequencies of any pair of species, e.g. $\Omega_3 < \omega < \Omega_2$ or $\Omega_2 < \omega < \Omega_1$. (We assume $\Omega_3 < \Omega_2 < \Omega_1$ without loss of generality.) As an example of relevance to our DIII-D experiment, assume the first species is hydrogen, the second is deuterium (and any fully stripped impurities with $Z/A = 1/2$), and the third species is carbon ions that have lost their outer electrons but retain their 1s shell: $Z_1/A_1 = 1$, $Z_2/A_2 = 1/2$, and $Z_3/A_3 = 4/12 = 1/3$. Equation (5) reduces to

$$\frac{f_1}{1-\hat{\omega}}+\frac{f_2}{1-2\hat{\omega}}+\frac{f_3}{1-3\hat{\omega}}\simeq 1, \tag{7}$$

where $\hat{\omega}\equiv\omega/\Omega_1$ is the normalized cutoff frequency. There are two solutions, a predominately deuterium–carbon cutoff and a predominately hydrogen–deuterium cutoff. A similarity between the two-ion species plasma and the three-ion species plasma is that both resonance curves are below their respective cutoff curves. This reveals that the third species does not interfere directly with the hydrogen–deuterium cutoff–resonance couplet. The ratio mix of hydrogen at $f_1 = 30\%$, deuterium at $f_2 = 60\%$, and C^{+4} at $f_3 = 10\%$ results in the frequency structure illustrated in figure 4.

For the experimental results shown in section 4, the majority of our analysis assumes a two-species plasma. Much of the data were obtained in 'conditioning' plasmas immediately following a major vent, and so the impurity content of the plasma was relatively high. Figure 5 shows the effect of an admixture of C^{+4} impurity on the hydrogen–deuterium cutoff frequency. Even if the C^{+4} accounts for 20% of the electron density (an unrealistically high value), the hydrogen–deuterium cutoff only shifts ~3%; so the effect of additional impurities is negligible compared with other uncertainties in the analysis.

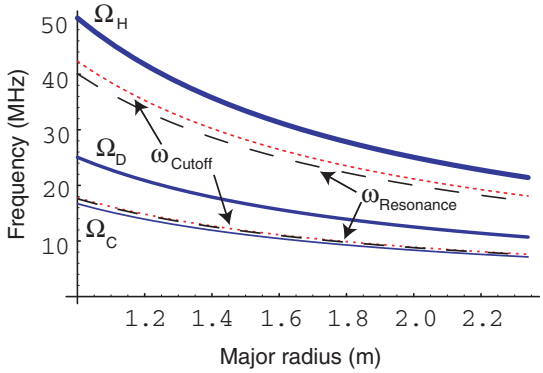

Figure 4. The ion–ion hybrid cutoffs (· · · · · ·), ion–ion hybrid resonances (- - - -), and C^{+4}, deuterium, and hydrogen cyclotron frequencies vs major radius, R, in a plasma with hydrogen, deuterium, and partially stripped carbon ions. One hybrid couplet (cutoff and resonance) lies between the hydrogen and deuterium cyclotron frequencies, and the other couplet lies between the deuterium and C^{+4} cyclotron frequencies.

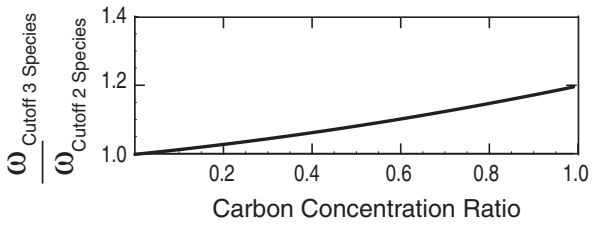

Figure 5. Fractional change in the upper (hydrogen–deuterium) cutoff frequency relative to a pure deuterium–hydrogen plasma vs C^{+4} concentration, f_C, for $f_H/f_D = 2$.

Thermal corrections to cold plasma theory are also unimportant. The warm-plasma dispersion relation for perpendicular propagation is (equation (13.43) of [13]),

$$Wn^4 - Sn^2 + RL = 0, \tag{8}$$

where $W \simeq 0.5[\beta_1(\omega^2/(\Omega_1^2 - \omega^2) - \omega^2/(4\Omega_1^2 - \omega^2)) + \beta_2(\omega^2/(\Omega_2^2 - \omega^2) - \omega^2/(4\Omega_2^2 - \omega^2))]$ is the new term associated with thermal effects. (Here, β_1 and β_2 are the ratio of perpendicular kinetic pressure to magnetic pressure for the two ion species.) The solution of equation (8) for a representative case is shown in figure 6. For a LFS launch the thermal corrections are utterly negligible: the location of the cutoff is unchanged and the wave velocity is barely altered. In contrast, thermal effects do move the resonance layer closer to the inner wall, and so they could have an effect during a HFS launch in a hot plasma. However, in our HFS experiments, the ion beta is very low (∼0.2%), and so the cold plasma theory suffices.

3. Apparatus

The experiments are performed in the DIII-D tokamak [20]. The launching and receiving antennas are one-turn toroidal loops with cross-sectional areas of 8–17 cm^2; a modified graphite tile forms the plasma-facing portion of the loop [21]. These relatively small loops launch a broad wavenumber spectrum centred about $k_\parallel \simeq 0$ [22]; the toroidal orientation of the loop

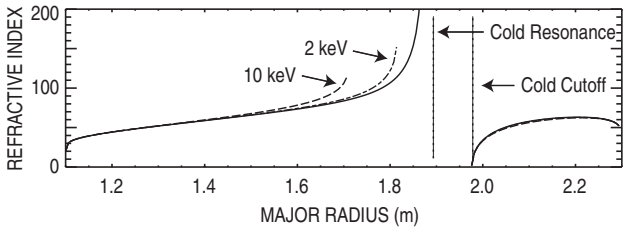

Figure 6. The index of refraction, n, vs major radius, R, for parameters typical of the LFS experiments (figure 12). The solid line is the cold-plasma approximation; the dashed and dash-dot lines are the solutions of equation (8) for central ion betas of 6% and 1.2%, respectively. ($\beta_H(0)+\beta_D(0) \simeq 0.6\%$ in the experiment.) The vertical dotted lines are the radii where equations (4) and (2) are satisfied.

implies that the fast wave is preferentially excited. The launching and receiving antennas are at nearly identical toroidal angles but are displaced poloidally by 35 cm for the LFS experiment and 57 cm for the HFS experiment (figure 1).

The superheterodyne signal processing for the reflectometer is the same as for the DIII-D ICRF density interferometer [21]. The reflectometer uses a 20 mW launch signal with a frequency of 14–23 MHz (changed shot-to-shot) and an intermediate frequency (IF) of 4 MHz. For simplicity and economy, a static frequency signal is employed, although a more sophisticated system would sweep in frequency on a 10–100 ms timescale to measure the spatial profile of f_H.

The IF signals received are mixed with a pair of reference IF signals with phase shifts of 0° and 90° to determine the amplitude and phase. The signals at the difference frequency are (nearly) dc voltages that represent the X and Y phase components. Plotting X vs Y yields the phase of the data signal. When this plot is repeated over time, the changing phase forms loops. These loops represent a change in phase of the launched wave as it travels through the plasma. The resulting clockwise or counter-clockwise loops (positive or negative phase change) correspond to an increase or decrease in hydrogen concentration according to whether a LFS or HFS launch is used (table 1).

Several steps are required to relate the measured phase, φ, to the hydrogen concentration. The first step is to reconstruct the plasma equilibrium from magnetics measurements using the EFIT code [23]. Next, Thomson scattering [24] and CO_2 interferometer [25] measurements of the electron density, n_e, are mapped onto the equilibrium. A value of hydrogen concentration, f_H, is assumed, and then profiles of the index of refraction, n, are calculated from the known values of ω, $\boldsymbol{B}$, and n_e. The wave is assumed to travel from the launching antenna to the IIHCL and then bounce back to the receiving antenna. Although the actual wavefronts refract as they traverse the plasma, analysis reveals that if refraction is included the inferred hydrogen concentration changes less than 1%, and so the rays are approximated as straight lines from the antennas to the IIHCL (figure 1). Since the index of refraction along the wave path is known, the expected phase, θ, is simply $(\omega/c)\int n\,\mathrm{d}l$, where c is the speed of light. The value of f_H is iterated until the calculated phase, θ, agrees with the measured phase, φ.

This procedure assumes the validity of a ray treatment, which is suspect for such long wavelengths. To test this assumption, the phase is calculated with a one-dimensional full-wave code that can treat a cutoff–resonance couplet [26]. The profile of n employed in the code is the index of refraction along the assumed ray path. For a launch from the LFS, the inferred f_H changes an average of 3%, which is comparable with other experimental uncertainties. On the

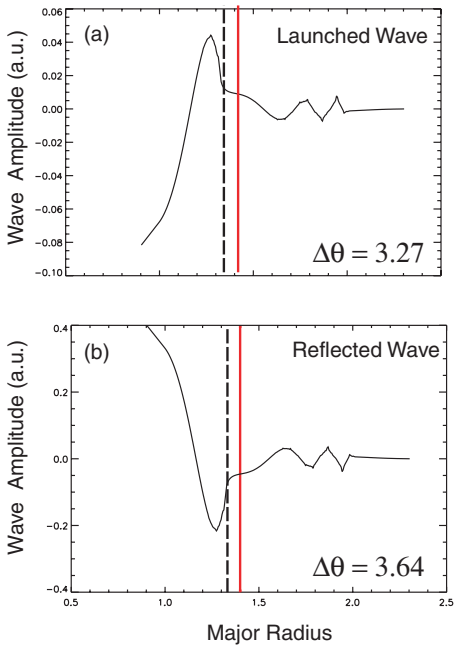

Figure 7. Solutions of the one-dimensional full-wave code [26] for the amplitude of (*a*) a wave that travels from the HFS midplane antenna to the resonance–cutoff couplet and for (*b*) a wave that travels from the lower HFS antenna to the resonance–cutoff couplet. The index of refraction along the wave path is for $f_{\mathrm{H}} = 44\%$ in a discharge similar to the one shown in figure 9. The solid vertical line indicates the cutoff layer, and the dashed vertical line indicates the resonance layer. The phase change (in radians), $\Delta\theta$, between the antenna and the cutoff layer is given.

other hand, for waves launched from the HFS, the full-wave treatment is indispensable since the WKB treatment breaks down at the resonance. In this case, we use n along the ray paths to calculate the phase for the incoming and outgoing waves, assuming that the wave reflects from the cutoff layer after tunnelling through the resonance (figure 7).

One complication that arises from launching a static frequency is that only the change in phase, $\Delta\varphi$, is measured between two times. To make a quantitative measurement, a calibration phase (and corresponding f_{H}) is required. In some cases, this calibration point can be obtained from the time evolution of the signal. For certain values of f_{H} and ω, the cutoff layer is beyond the plasma boundary. Under these conditions, no coherent reflected signal is received by the diagnostic. As f_{H} evolves, the cutoff layer enters the plasma and the signal becomes much less noisy, indicating reception of a reflected wave. If we assume that this occurs when the IIHCL is at the plasma edge, the phase at this instant provides a calibration point for the diagnostic. This technique is employed in the analysis of the LFS experiment in section 4. For the HFS experiment, the appearance and disappearance of a coherent signal is attributed to other factors (discussed further below), and so the calibration point is taken from a spectroscopic determination of f_{H}.

The hydrogen concentration inferred from reflectometry is compared with data from two independent techniques. One is the ratio of H_α to D_α light measured spectroscopically. For the HFS experiment, divertor light was measured with 62 ms temporal resolution. For the LFS experiment, scattered edge light was measured with 10 ms temporal resolution. In both cases, the ratio of the light in the unshifted H_α and D_α peaks is assumed to equal the ratio of ion densities, $n_{\mathrm{H}}/n_{\mathrm{D}}$.

The other diagnostic measures the central deuterium density from the jump in the neutron rate when a 2 ms long deuterium beam pulse is injected into the plasma [9]. The analysis utilizes measurements of the central electron density to infer the deuterium concentration, n_D/n_e. The hydrogen concentration is assumed to be $f_H = 1 - n_D/n_e - Z_C n_C/n_e$, where $Z_C n_C/n_e \simeq 10\%$ represents the fraction of electrons neutralized by fully stripped carbon impurities.

4. Experimental results

The HFS experiment was conducted during the first 500 ms of a set of discharges that studied the dependence of the H-mode pedestal width on ion species [27]. The LFS experiments were conducted during plasma conditioning discharges following a major vent during the beginning of the 2003 experimental campaign. In both cases, hydrogen gas was puffed into the tokamak early in the discharge. Since DIII-D operates normally in deuterium, an unknown quantity of deuterium is released from the walls during the discharge. Additional fuelling is provided by hydrogen neutral beam injection during the HFS experiment and deuterium neutral beam injection during the LFS experiment.

The same ICRF equipment was previously used at 100 MHz to make interferometric measurements of the plasma density [21]. In that study, sensible signals (termed 'tracking') were only received when the gaps between the plasma and the antennae were small. Based on that experience, favourable plasma shapes were employed early in the discharge for the experiments reported here. The toroidal field was 1.2 and 2.0 T for the HFS experiment and 1.9–2.1 T for the LFS experiment.

Figure 8 shows data from the LFS experiments. In this discharge, hydrogen gas is puffed from 300 to 700 ms during the current ramp. Evidence of 'tracking' begins around 300 ms, but the signal is noisy until 500 ms. The noisy signal may be caused by the relatively large antenna gaps or by poor plasma stability (many minor disruptions are evident on the central soft x-ray signals) or both. Just before beam injection commences at 500 ms, a minor disruption occurs; thereafter, the signal becomes less noisy as the outer plasma edge grows closer to the antennas and plasma stability improves. The phase inferred from the X and Y components first decreases while hydrogen gas is puffed into the discharge and then abruptly reverses direction when the gas puff ceases and deuterium particle sources predominate. The observed phase dependence agrees with the expected behaviour (table 1). On a finer scale, changes in phase correlate with sawteeth observed on central soft x-ray signals. At a sawtooth, the density profile flattens and rapid particle transport occurs, both of which can alter the wave phase through changes in the index of refraction.

Data from the HFS experiment are shown in figure 9. Although the antenna gaps are smaller than in the LFS experiment, the received signals are an order of magnitude smaller (with the same equipment) and intelligible 'tracking' is only observed for $\sim$100 ms. In one comparison on the same day with similar discharges, tracking was readily observed with a LFS launch but was unobservable during a HFS launch. As expected (table 1), when tracking is observed, the phase change is opposite to that in the LFS experiment during the hydrogen gas puff. Representative polar plots for both the HFS and LFS experiments are shown in figure 10.

The shape of the plasma boundary for both the experiments is illustrated in figure 11. The likely reason for the diagnostic failing when the antenna–plasma gap is large is that the wave is evanescent in the low-density 'vacuum' region near the vessel wall [21, 28]. Representative electron density and temperature profiles for the LFS experiments are shown in figure 12.

In some discharges in the LFS experiments, the hydrogen gas puff began at 400 ms rather than 300 ms. In these cases, the phase evolution delayed 100 ms, as expected. As a further test, the frequency of the launched wave was varied between 14 and 22 MHz. Initially, when the

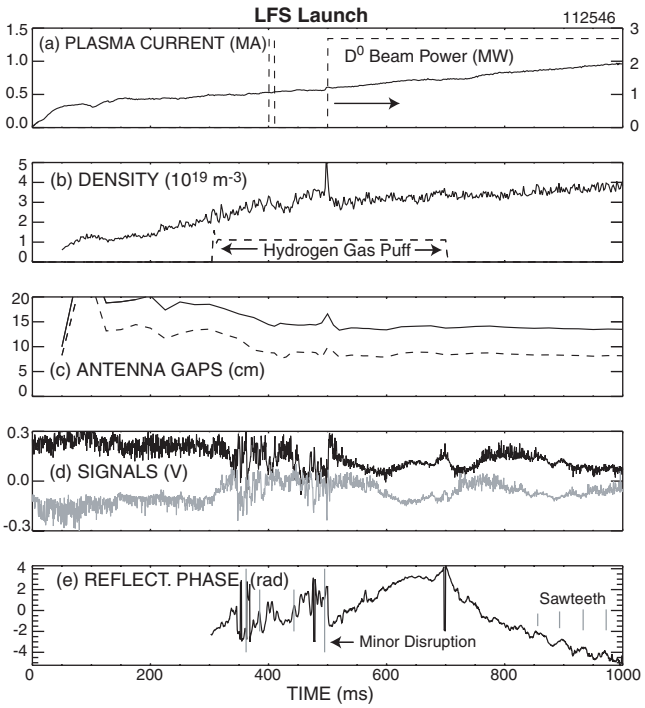

Figure 8. Time evolution of (*a*) plasma current and injected beam power of 80 keV deuterium neutrals, (*b*) line-average electron density and timing of the hydrogen gas puff, (*c*) gaps between the last-closed flux surface and the two outer-wall graphite tile antennas, (*d*) X and Y mixed signals of the reflectometer diagnostic, with a dc offset introduced for clarity, and (*e*) the inferred reflectometer phase (after 3.5 ms boxcar smoothing). The grey vertical lines indicate vertical drops in a central soft x-ray signal, with the length of the line proportional to the fractional change in the signal. Increasing phase in this figure corresponds to a counter-clockwise rotation in figure 10. $B_{\mathrm{T}} = 2.1\,\mathrm{T}$, $\omega/(2\pi) = 21\,\mathrm{MHz}$, LFS launch.

hydrogen concentration is low, the launch frequency, ω, is lower than the ion–ion hybrid cutoff frequency, $\omega_{\mathrm{cutoff}}(R)$, everywhere in the plasma. Tracking commences when $\omega = \omega_{\mathrm{cutoff}}$ at the plasma edge. As expected, phase tracking began earlier in discharges with higher launch frequencies (figure 13).

Figure 14 shows the hydrogen concentration inferred by three independent diagnostics for one of the discharges in the LFS experiment. In this discharge, phase tracking first occurs 4 ms after the hydrogen gas puff begins, indicating that the IIHCL entered the plasma at this time. This observation provides a calibration phase for the reflectometer signal, and so the subsequent evolution of f_{H} is determined from the reflectometer signals alone. All three diagnostic techniques record a significant increase in hydrogen concentration, f_{H}, when the hydrogen gas puff begins at 300 ms. Like the reflectometer, the $\mathrm{H}_\alpha : \mathrm{D}_\alpha$ spectroscopic diagnostic records a decrease in hydrogen concentration at the end of the hydrogen gas puff at 700 ms. (The beam blip diagnostic is unavailable after steady beam injection begins at 500 ms.) In addition to these general trends, the data suggest that f_{H} varies spatially. The spectroscopic diagnostic measures f_{H} in the plasma boundary, the reflectometer diagnostic measures f_{H} at an intermediate minor radius, and the beam blip diagnostic measures f_{H} at the plasma centre. When the hydrogen gas puff begins, f_{H} first increases at the plasma boundary (spectroscopic signal), then at intermediate radii (reflectometer signal), then finally at the plasma centre

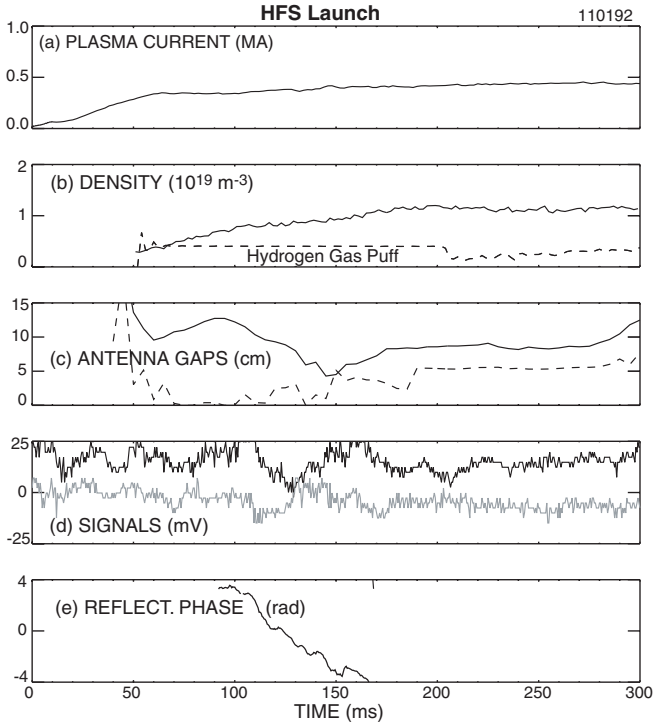

Figure 9. Time evolution of (*a*) plasma current, (*b*) line-average electron density and timing of the hydrogen gas puff, (*c*) gaps between the last-closed flux surface and the two inner-wall graphite tile antennas, (*d*) X and Y mixed signals of the reflectometer diagnostic, with a dc offset introduced for clarity, and (*e*) the inferred reflectometer phase (after 3.5 ms boxcar smoothing). Increasing phase corresponds to a counter-clockwise rotation in figure 10. $B_{\mathrm{T}} = 1.2\,\mathrm{T}$, $\omega/(2\pi) = 17.5\,\mathrm{MHz}$, HFS launch.

(beam blip signal). As the concentration approaches its asymptotic value at 500 ms, however, the situation is reversed: the central beam blip signal is largest, followed by the intermediate reflectometer signal, with the boundary spectroscopic signal lowest. With the differing spatial sensitivities taken into account, the data in figure 14 provide convincing evidence that the hydrogen concentration inferred from the reflectometer measurements is valid.

Several factors contribute to the uncertainty in the determinations of f_{H} in figure 14. The largest random error is associated with uncertainties in the electron density profile and the mapping of the available density measurements onto the equilibrium. Possible systematic errors include uncertainty in the equilibrium reconstruction and the use of a single ray to calculate the phase change rather than a full-wave treatment. Another source of systematic error is the assumption that the hydrogen and deuterium concentrations are spatially constant. If the hydrogen concentration is assumed to decrease linearly with minor radius, as suggested by the data, the value of f_{H} inferred from the reflectometer data increases about 10% (from 30% to 33%, for example). For the spectroscopic measurement, a useful estimate of the random error is obtained from an ensemble of adjacent times in the stationary phase of the discharge. Comparison with another spectrometer channel yields a similar estimate. A possible systematic error is the assumption that atomic hydrogen and deuterium radiation are proportional to n_{H} and n_{D}. Another source of systematic error is the estimate of the impurity concentration, which was not measured in this discharge. For the beam blip measurement, uncertainties in

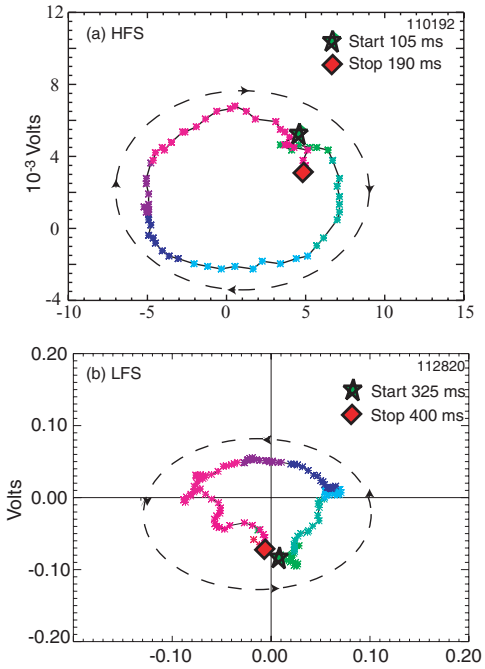

Figure 10. (*a*) Phase-space diagram between 105 and 190 ms for the X–Y mixed signals shown in figure 9. For a HFS launch, a clockwise rotation is expected when the hydrogen concentration increases. (*b*) Phase-space diagram between 325 and 400 ms for the X–Y mixed signals shown in figure 8. For a LFS launch, a counter-clockwise rotation is expected when the hydrogen concentration increases. (The signals are smoothed.)

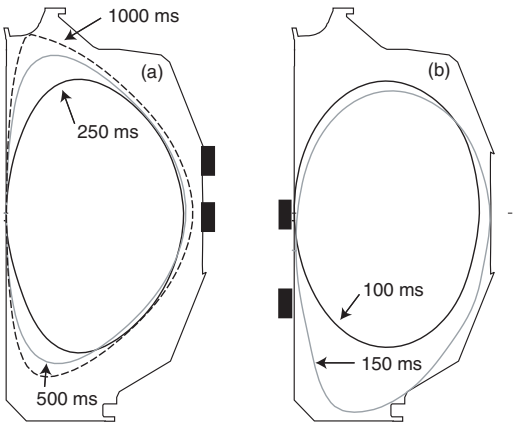

Figure 11. Elevation of the DIII-D vessel showing the shape of the last-closed flux surface (*a*) at 250, 500, and 1000 ms in the discharge of figure 8 and (*b*) at 100 and 150 ms in the discharge of figure 9. The locations of the antennas are indicated by the black rectangles.

the fitting of the neutron signal and in the electron density contribute nearly equally to the relative uncertainty in $n_{\mathrm{D}}/n_{\mathrm{e}}$. Systematic errors in the neutron calibration affect the absolute uncertainty. The largest systematic uncertainty is probably the impurity concentration, which is needed to relate $n_{\mathrm{D}}/n_{\mathrm{e}}$ to $n_{\mathrm{H}}/n_{\mathrm{e}}$.

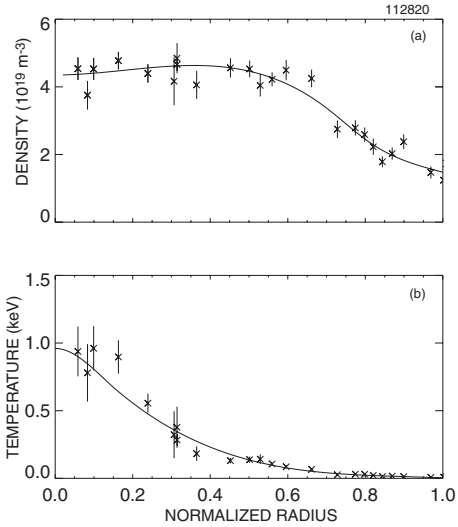

Figure 12. Thomson scattering measurements of (*a*) the electron density, n_e, and (*b*) the electron temperature, T_e, vs minor radius at 700 ms in the discharge shown in figure 14. The solid lines show the fits to the data that are used to calculate the index of refraction; CO_2 interferometer measurements of the line-average electron density are incorporated in the fitting procedure for n_e. The minor radius is the normalized square root of the toroidal flux.

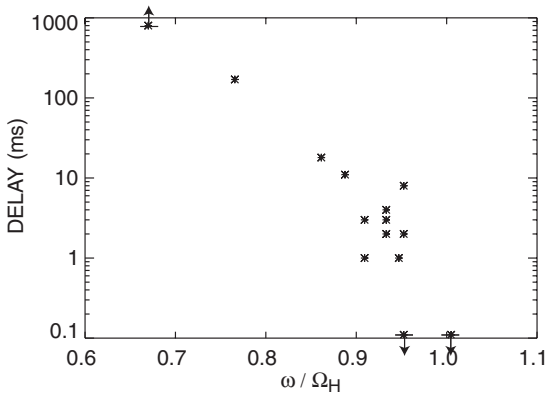

Figure 13. Temporal delay between the beginning of the hydrogen gas puff and the change in slope of the reflectometer phase (onset of tracking) as a function of the ratio of the launch frequency, ω, to the hydrogen cyclotron frequency at the outer edge of the plasma for all the LFS discharges with valid data. The downward arrows indicate tracking that began before the gas puff; the upward arrow indicates a discharge without tracking. A typical uncertainty in the delay is 2 ms.

Figure 15(*a*) compares the f_H-value inferred from the reflectometer diagnostic with the H/(H + D) ratio measured by the spectroscopic diagnostic. In this figure, the reflectometer data are restricted to the three shots with the outermost cutoff layers, and so the two diagnostics measure close to the same spatial location. The correlation between the measurements is high (a correlation coefficient of $r = 0.85$). If all the available reflectometer data are compared with the spectroscopic measurements (figure 15(*b*)), the correlation is much weaker (correlation coefficient $r = 0.54$). This variability is caused by the different spatial sensitivities of the two measurements. The reflectometer measures variable depths into the plasma that ultimately

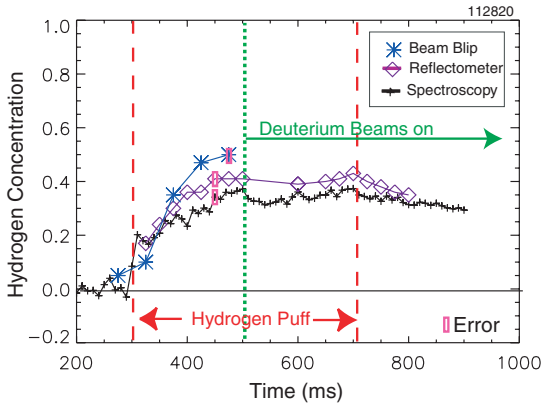

Figure 14. Time evolution of the hydrogen concentration inferred from the beam blip neutron diagnostic (∗), the ion–ion hybrid reflectometer diagnostic (◊), and the H_α/D_α spectroscopic diagnostic (+). Typical random error bars for each diagnostic are shown. A hydrogen gas puff begins at 300 ms and ends at 700 ms; deuterium beam injection begins at 500 ms. To relate the beam blip and spectroscopic diagnostics to f_H, a constant carbon density of $1.6 \times 10^{12}\,\mathrm{cm}^{-3}$ is assumed. $B_T = 1.9\,\mathrm{T}$, $\omega/(2\pi) = 19.5\,\mathrm{MHz}$, LFS launch.

depend on the parameters ω and f_H, while the spectroscopic diagnostic measures boundary light. The interior reflectometer measurements usually measure a larger value of f_H than the spectroscopic measurements, suggesting some peaking of the hydrogen concentration profile (see also figure 14).

Figure 15(*c*) compares the reflectometer measurement of n_H/n_e with the deuterium concentration, n_D/n_e, inferred from the beam blip diagnostic. As expected, these quantities are inversely related, with a correlation coefficient of $r = -0.83$; the data approximately satisfy the relation $f_H + f_D \simeq$ constant.

Independent confirmation of the HFS measurements is hampered by the short duration of the reflectometer measurements and by the poor temporal resolution of the available spectroscopic and beam blip data. The inferred increase in hydrogen concentration during tracking, $\Delta f_H = \Delta n_H/n_e$, does correlate with the density rise, $\Delta n_e/n_e$ (figure 16), which makes sense, since the hydrogen gas puff is the primary particle source during this phase of the discharge.

5. Summary and conclusions

Numerous features of the LFS data indicate that the waves reflect off the IIHCL as illustrated in figure 1.

- The temporal evolution correlates with the timing of the hydrogen gas puff and with sawtooth events (figure 8).
- The signal varies with ω in the expected manner (figure 13).
- The inferred concentration agrees quantitatively with independent measurements (figures 14 and 15) within experimental error when the different spatial sensitivities of the three techniques are considered.

The maximum and minimum observed hydrogen concentrations during this experiment are 3% and 67%, respectively. The deepest penetration depth is 0.60 m (near the magnetic axis), and the duration of the measurement approaches 1 s.

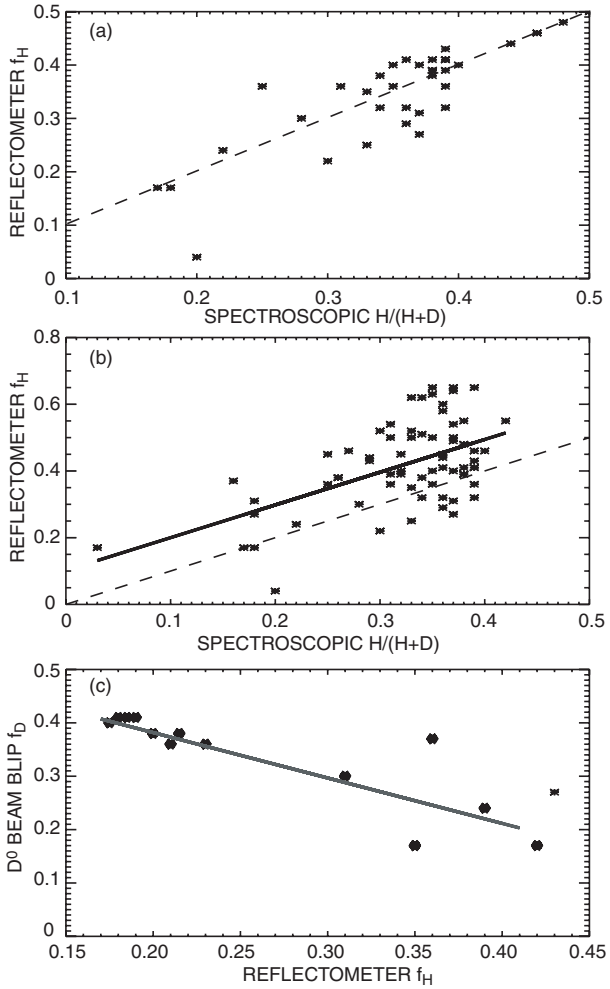

Figure 15. (*a*) Reflectometer hydrogen concentration measurements vs spectroscopic H/(H + D) ratio for the three discharges where the IIHCL was closest to the plasma boundary. The dashed line indicates perfect agreement in a plasma with no impurities. (*b*) Comparison of the reflectometer and spectroscopic measurements for all the available discharges. The solid line is from a least-squares fit to the data. (*c*) Deuterium concentration inferred from the neutron beam blip technique vs reflectometer hydrogen concentration measurements for all the available LFS data. The solid line is from a least-square fit to the data.

During a HFS launch, signals that appear to reflect off the IIHCL are also detected. The amplitude of these signals is an order of magnitude smaller than for a LFS launch; tracking only lasts ∼0.1 s. The phase change during the hydrogen gas puff is opposite to the phase change during a LFS launch, as expected (figure 10). When interpreted as reflected fast waves, the signals yield sensible values for the hydrogen concentration (figure 16), suggesting that some of the wave energy tunnels through the resonance layer to be reflected from the cutoff layer. The inferred hydrogen concentrations vary between 51% and 81%, and the deepest penetration depth is 0.4 m.

These are promising proof-of-principle results, but a number of issues remain unaddressed. One important issue is the loss of signals in unfavourable shapes with large plasma–antenna

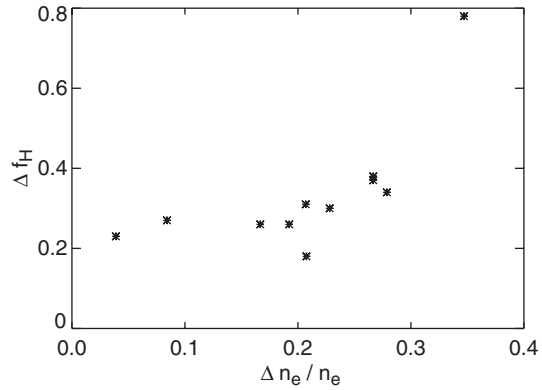

Figure 16. Change in hydrogen concentration during tracking vs the fractional increase in electron density during the same time window for all the available HFS discharges. (Hydrogen gas was puffed throughout the tracking period.)

gaps. A possible solution is to launch more power than the modest 20 mW employed in this experiment, but if spurious signals from 'cross-talk' or other waves predominate, additional power will not overcome the difficulties associated with a large evanescent layer. Since the temperatures in these experiments are a relatively modest 1 keV, another potential issue is hot-plasma effects in a burning plasma, but theory suggests these effects are insignificant for a LFS launch (figure 6). A further limitation is that, for the purposes of this diagnostic, all ions with the same charge-to-mass ratio constitute a 'species', and so deuterium and alpha ash will both contribute to the 'deuterium' density in a deuterium–tritium reactor. Nevertheless, because of its technical simplicity, this diagnostic could help optimize the fusion reaction rate and the efficiency of ICRF heating in a burning plasma experiment. In addition, with the use of multiple receiving antennas and a swept launching frequency, profile measurements could find wide utility in hydrogenic particle transport studies and in studies of the effect of the isotopic composition on energy transport.

Acknowledgments

We would like to thank R Boivin, R Fisher, A Hyatt, D Whyte and the DIII-D team for their assistance. This work was supported by US DOE subcontract SC-G903402 of US DOE contract DE-AC03-99ER54463.

References

[1] Anashin M *et al* 1971 *Sov. Phys.—JETP* **33** 1127
[2] Skinner C H, Stotler D P, Adler H and Ramsey A T 1995 *Rev. Sci. Instrum.* **66** 646
[3] Ivanov N V, Kovan I A and Sokolov Y A 1976 *Sov. Phys.—JETP* **24** 316
[4] Afanasyev V I *et al* 2003 *Rev. Sci. Instrum.* **74** 2338
[5] Afrosimov V V, Berezovskii E L, Izvozchikov A B and Petrov M P 1980 *Sov. J. Plasma Phys.* **6** 133
[6] ITER Physics Expert Group on Diagnostics 1999 *Nucl. Fusion* **39** 2541
[7] Afanasyev V I, Gondhalekar A and Kislyakov A I 2000 On the possibility of determining the radial profile of hydrogen isotope composition of jet plasmas, and of deducing radial transport of the isotope ions *Technical Report* JET-R(00)04, JET, 2000
[8] Strachan J D, Chrienk R E and Heidbrink W W 1983 *J. Vac. Sci. Technol.* A **1** 811
[9] Heidbrink W W, Kim J and Groebner R J 1988 *Nucl. Fusion* **28** 1897

[10] Heidbrink W W 1986 *Nucl. Instrum. Methods Phys. Res.* A **248** 491
[11] Efthimion P C *et al* 1995 *Phys. Rev. Lett.* **75** 85
[12] Ikezi H, Degrassie J S, Pinsker R I and Snider R T 1997 *Rev. Sci. Instrum.* **68** 478
[13] Stix T H 1992 *Waves in Plasmas* (New York: American Institute of Physics)
[14] Buchsbaum S J 1960 *Phys. Fluids* **3** 418
[15] Swanson D G 1985 *Phys. Fluids* **28** 2645
[16] Equipe TFR 1983 *Plasma Physics and Controlled Nuclear Fusion Research 1982* vol 2 (Vienna: IAEA) p 17
[17] Ngan Y C and Swanson D G 1977 *Phys. Fluids* **20** 1920
[18] Stix T H 1985 *Nucl. Fusion* **15** 737
[19] Majeski R, Phillips C K and Wilson J R 1994 *Phys. Rev. Lett.* **73** 2204
[20] Luxon J L 2002 *Nucl. Fusion* **42** 614
[21] Watson G W and Heidbrink W W 2003 *Rev. Sci. Instrum.* **74** 1605
[22] Watson G W 2003 Ion species mix and ion density measurements using radio frequency waves *PhD Thesis* University of California, Irvine
[23] Lao L L, St John H, Stambaugh R D, Kellman A G and Pfeiffer W P 1985 *Nucl. Fusion* **25** 1611
[24] Carlstrom T N *et al* 1992 *Rev. Sci. Instrum.* **63** 4901
[25] Carlstrom T N, Ahlgren D R and Crosbie J 1998 *Rev. Sci. Instrum.* **59** 1063
[26] Kramer G J, Nazikian R and Valeo E 2002 *Plasma Phys. Control. Fusion* **44** L11
[27] Groebner R J *et al* 2003 *Nucl. Fusion* **43** at press
[28] Mayberry M J *et al* 1990 *Nucl. Fusion* **30** 579